Physics Letters A 380 (2016) 3871–3875

Contents lists available at ScienceDirect

Physics Letters A

www.elsevier.com/locate/pla

# Mitigation of radiation-pressure-induced angular instability of a Fabry–Perot cavity consisting of suspended mirrors

Koji Nagano [a,*], Yutaro Enomoto [a], Masayuki Nakano [a], Akira Furusawa [b], Seiji Kawamura [a]

[a] KAGRA Observatory, Institute for Cosmic Ray Research, The University of Tokyo, 5-1-5 Kashiwa-no-Ha, Kashiwa, Chiba 277-8582, Japan
[b] Department of Applied Physics, School of Engineering, The University of Tokyo, 7-3-1 Hongo, Bunkyo-ku, Tokyo 113-8656, Japan

ARTICLE INFO

*Article history:*
Received 14 July 2016
Received in revised form 20 September 2016
Accepted 30 September 2016
Available online 3 October 2016
Communicated by P.R. Holland

*Keywords:*
Fabry–Perot
Anti-spring effect
Optomechanical
Torque
Radiation pressure
Feedback control

ABSTRACT

To observe radiation pressure noise in optical cavities consisting of suspended mirrors, high laser power is necessary. However, because the radiation pressure on the mirrors could cause an angular anti-spring effect, the high laser power could induce angular instability to the cavity. An angular control system using radiation pressure as an actuator, which was previously invented to reduce the anti-spring effect for the low power case, was applied to the higher power case where the angular instability would occur. As a result the angular instability was mitigated. It was also demonstrated that the cavity was unstable without this control system.



## 1. Introduction

Second-generation ground-based interferometric gravitational wave detectors, for example Advanced LIGO [1], Advanced Virgo [2], GEO-HF [3], and KAGRA [4], are operated or constructed. Among these gravitational wave detectors, Advanced LIGO detected gravitational waves and established gravitational wave astronomy [5]. The design sensitivities of these second-generation interferometric gravitational wave detectors are limited mostly by quantum noise. Thus, quantum noise must be reduced in order to obtain better sensitivities for developing gravitational wave astronomy [6–13].

Quantum noise consists of radiation pressure noise and shot noise [14]. To demonstrate the technique of reducing quantum noise, especially radiation pressure noise, it is necessary to perform a measurement limited by radiation pressure noise. In order to observe radiation pressure noise, i.e. in order to enhance radiation pressure noise and reduce the other noises, high finesse Fabry–Perot cavities consisting of suspended tiny mirrors are useful [15]. Such cavities are also used in experiments for other purposes, for example exploring macroscopic quantum mechanics [16].

However, the radiation pressure of the resonant light of the cavity could cause an angular instability of the cavity depending on the geometries of the cavity [17]. The angular instability occurs due to the angular optical anti-spring effect generated by the radiation pressure. The radiation-pressure-induced angular instability of the optical cavity has been observed in experiments with various scale mirrors [18–20]. This angular instability is more serious in experiments which require higher laser power for observing radiation pressure noise.

To mitigate the radiation-pressure-induced angular instability, angular motion of the mirrors of the cavity should be controlled to reduce the angular anti-spring effect which induces the angular instability of the cavity. The angular control technique has been demonstrated in experiments with large size mirrors, for example 10 kg mirrors [19]. For experiments with tiny mirrors which do not have conventional actuators because of spatial constraints, the new angular control technique using radiation pressure as an actuator was invented to reduce the angular optical anti-spring effect [21,22]. The authors successfully demonstrated this angular control technique by observing a reduction of the optical anti-spring effect [22]. However, previous experiments were carried out in a low laser power regime where the cavity would not be unstable even without the angular control system because of the low laser power. That is, the angular optical anti-spring effect is small. In other words, it was not yet verified if this angular control system

* Corresponding author.
*E-mail address:* knagano@icrr.u-tokyo.ac.jp (K. Nagano).

http://dx.doi.org/10.1016/j.physleta.2016.09.056
0375-9601/

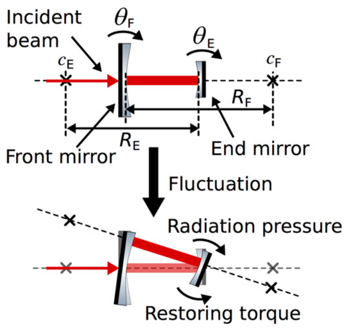


**Fig. 1.** Schematic view of the cavity and the angular optical anti-spring effect generated by radiation pressure. The front and end mirrors are suspended. $c_{F(E)}$, $R_{F(E)}$, and $\theta_{F(E)}$ are the center of curvature, the radius of curvature (RoC), and angle of the front (end) mirror, respectively. Positive directions of $\theta_F$ and $\theta_E$ are defined as clockwise direction.

works also for the higher power case where the angular instability of the cavity would occur without this control system.

In order to observe the radiation pressure noise in our experimental setup, the intracavity power should be high enough such that the angular instability would occur. Although the authors have shown feasibility of the angular-control scheme [22], it is still required to demonstrate the mitigation of the angular instability by this angular control system under high laser power condition where the cavity would be unstable without this angular control system.

## 2. Review of the angular optical anti-spring effect generated by radiation pressure and its reduction

The radiation-pressure-induced angular anti-spring effect of a suspended optical cavity as shown in Fig. 1 is explained in terms of the equation of rotational motion of the mirrors composing the cavity [23,24]. The equation of rotational motion of the end mirror is obtained from Fig. 1 as

$$I_E\ddot{\theta}_E = -(k_{\mathrm{mech}} - k_{\mathrm{RP}})\theta_E - k'_{\mathrm{RP}}\theta_F, \tag{1}$$
$$\left(\mathcal{L} = \frac{L}{1-g_F g_E},\ k_{\mathrm{RP}} = \frac{2P_{\mathrm{int}}}{c}\mathcal{L}g_F,\ k'_{\mathrm{RP}} = \frac{2P_{\mathrm{int}}}{c}\mathcal{L}\right),$$

where $I_E$ is the moment of inertia (MoI) for an axis of rotation passing through the center of the end mirror, $k_{\mathrm{mech}}$ is the angular mechanical spring constant of the end mirror, $k_{\mathrm{RP}}$ is the angular optical anti-spring constant of the end mirror caused by the radiation pressure of the resonant light on the end mirror, $L$ is the cavity length, and $g_F$ and $g_E$ are the g-parameters, which are defined as $g_i = 1 - L/R_i$ ($i = $ F, E), for the front and end mirrors, respectively, $P_{\mathrm{int}}$ is intracavity power, and $c$ is the speed of light. The radiation pressure formed as $k_{\mathrm{RP}}$ applied to the end mirror works as optical antispring. Therefore if $k_{\mathrm{RP}}$ increases, in other words the intracavity power increases, the rotational resonant frequency of the end mirror decreases. Moreover, if $k_{\mathrm{RP}}$ is larger than $k_{\mathrm{mech}}$, the cavity would be unstable. The authors demonstrated the decrease of the rotational resonant frequency caused by the angular optical anti-spring effect [24].

In order to reduce the optical anti-spring effect inducing the angular instability of the cavity, the angular control system that the angle of the end mirror is fed back to the angle of the front mirror was invented [21]. If the front mirror is much heavier than the end mirror and the radiation pressure applied to the front mirror is negligible, the angular control system is explained by the block diagram shown in Fig. 2. In the angular control system, the displacement of the beam spot on the end mirror is fed back to the angular motion of the front mirror. If the end mirror is suspended as a single pendulum, the transfer function from the torque applied to the end mirror to the angle of the end mirror, in other words the susceptibility of the end mirror, with the angular feedback control is obtained as

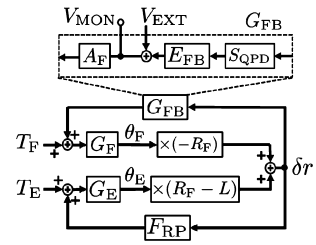


**Fig. 2.** Block diagram corresponding to the angular system of the cavity. Here, $T_F$ and $T_E$ are external torques applied to the front and end mirrors respectively, $\delta r$ is the displacement of the beam spot on the end mirror, $G_F$ and $G_E$ are mechanical susceptibilities of the angular motions of the front and end mirrors respectively, $F_{\mathrm{RP}}$ is the force applied to the end mirror cause by radiation pressure of the resonant light in the cavity, and $G_{\mathrm{FB}}$ is the transfer function from the displacement of the beam spot on the end mirror to the torque applied to the front mirror. $G_{\mathrm{FB}}$ can be divided into three components, $A_F$, $E_{\mathrm{FB}}$, and $S_{\mathrm{QPD}}$. $A_F$ is the coil-magnet actuator efficiency, $E_{\mathrm{FB}}$ is the transfer function of the electric circuit for yaw-mode control, and $S_{\mathrm{QPD}}$ is the sensitivity of the QPD. $E_{\mathrm{FB}}$ includes a variable gain amplifier. $V_{\mathrm{EXT}}$ and $V_{\mathrm{MON}}$ are excitation and monitor ports, respectively, which are used to measure $\delta r/V_{\mathrm{MON}}$.

$$\frac{\theta_E}{T_E} = \frac{1/4\pi^2 I_E}{-f^2 + \left[f_{\mathrm{mech}}^2 - \frac{(R_F-L)F_{\mathrm{RP}}}{4\pi^2 I_E(1+G_{\mathrm{FB}}G_F R_F)}\right] + \mathrm{i}\frac{f_{\mathrm{mech}}}{Q_{\mathrm{mech}}}f}, \tag{2}$$

where $f$ is the frequency, $F_{\mathrm{RP}}$ is given by $2P_{\mathrm{int}}/c$, $f_{\mathrm{mech}}$ is the mechanical rotational resonant frequency of the end mirror, and $Q_{\mathrm{mech}}$ is the mechanical Q-value of the rotational mode of the end mirror. When the angular control system is off, i.e. $G_{\mathrm{FB}} = 0$, the second term of the denominator in Eq. (2) is $f_{\mathrm{mech}}^2 - \frac{(R_F-L)F_{\mathrm{RP}}}{4\pi^2 I_E}$. That is, the rotational resonant frequency of the end mirror decreases because of the angular optical anti-spring effect. When the angular control system is on, the anti-spring effect is reduced by the angular feedback control. For example, if $|G_{\mathrm{FB}}G_F R_F| \gg 1$, the rotational resonant frequency of the end mirror decreased by the optical anti-spring effect, $\sqrt{f_{\mathrm{mech}}^2 - \frac{(R_F-L)F_{\mathrm{RP}}}{4\pi^2 I_E(1+G_{\mathrm{FB}}G_F R_F)}}$, would be the mechanical resonant frequency, $f_{\mathrm{mech}}$. The authors demonstrated experimentally that, using the angular feedback control, the rotational resonant frequency of the end mirror is restored toward its mechanical value [22].

## 3. Mitigation of the angular instability

The authors have already shown that the angular control system can reduce the effect of the angular optical anti-spring under the low laser power condition [22]. However, it is still necessary to demonstrate experimentally the mitigation of the angular instability. For this experimental demonstration, the angular control system using radiation pressure used in a previous experiment [22] to reduce the angular anti-spring effect under lower laser power condition discussed in Sec. 2 is applied to the higher power case.

### 3.1. Experimental setup

Fig. 3 shows our experimental setup. The properties of the cavity and its component mirrors are shown in Table 1. The end mirror is suspended in a double pendulum structure. The front mirror is suspended as a double pendulum and has a coil-magnet actuator for controlling the rotational motion and the cavity length. The laser source is a Nd:YAG laser of the 1064-nm wavelength. The power of the laser incident to the cavity can be adjusted between 7 mW and 100 mW by adjusting the half wave plate and

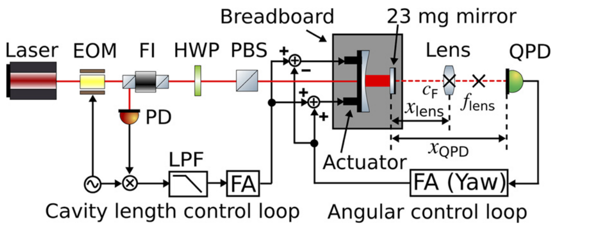


**Fig. 3.** Schematic view of our experimental setup. EOM is an electro-optic modulator; FI, a Faraday isolator; HWP, a half wave plate; PBS, a polarizing beam splitter; PD, a photo detector; QPD, a quadrant photo detector; LPF, an electronic low-pass filter; FA and FA (Yaw), an electronic filter amplifier for length control and angular control, respectively.

polarizing beam splitter. The intracavity power is determined by the power of the transmitted light measured by the sum of the quadrant photo detector (QPD) output, which is defined as $P_{\rm trans}$, and the calibration constant from the output voltage of the sum signal of the QPD to the intracavity power is $5.0 \pm 0.1$ W/V. The cavity length is controlled with Pound–Drever–Hall method using the light reflected by the cavity and the electro-optic modulator, which modulates the incident light [25]. After the cavity, for measuring the displacement of the beam spot on the tiny end mirror, the lens and the QPD are placed. The focal length of the lens is $f_{\rm lens} = (R_{\rm F} - L)/2$, and the positions of the lens and the QPD are $x_{\rm lens} = R_{\rm F} - L$, and $x_{\rm QPD} = 2(R_{\rm F} - L)$, respectively.

In this experiment, we measured the yaw mode of the end mirror since the rotational resonant frequency in the yaw mode of the mirrors is smaller than that in the pitch mode of the mirrors, i.e. the yaw mode would be unstable with lower laser power than the pitch mode. From here, the properties of the angular control system of our experimental setup are explained. For the better understanding of the angular control system, $G_{\rm FB}$ is divided into three components as shown in Fig. 2; the sensor (QPD) measuring the beam spot on the end mirror, $S_{\rm QPD}$, the electric circuit for the angular control system, $E_{\rm FB}$, and the actuator moving the front mirror, $A_{\rm F}$. The yaw-mode mechanical susceptibility of the end mirror is given by the single pendulum susceptibility and the rotational resonant frequency of the end mirror, $f_{\rm mech}$, is 2.62 Hz and the Q-value, $Q_{\rm mech}$, is 6.7. The reason why the end mirror can be considered to be single pendulum structure is that the higher rotational resonant frequency of the end mirror is about 11 Hz and the frequency is much higher than the measurement band, between 0.5 Hz and 2.6 Hz. The yaw-mode transfer function of the front mirror from the voltage applied to the coil-magnet actuator to the angle of the front mirror is measured as

$$A_{\rm F} G_{\rm F} = \frac{1}{4\pi^2} \sum_{n=1}^{2} \frac{a_n}{-f^2 + f_n^2 + {\rm i}\frac{f_n}{Q_n} f}, \tag{3}$$

where $A_{\rm F}$ is the coil-magnet actuator efficiency of yaw mode, $a_1 = 0.214\ {\rm rad\,Hz^2/V}$, $f_1 = 2.59$ Hz, $Q_1 = 3.70$, $a_2 = 0.418\ {\rm rad\,Hz^2/V}$, $f_2 = 16.2$ Hz, and $Q_2 = 49$. The transfer function of the electric circuit for the yaw-mode control system is designed as

$$E_{\rm FB} = E_{\rm DC} \frac{1 + {\rm i}\frac{f}{f_{\rm a}}}{\left(1 + {\rm i}\frac{f}{f_{\rm b}}\right)\left(1 + {\rm i}\frac{f}{f_{\rm c}}\right)}, \tag{4}$$

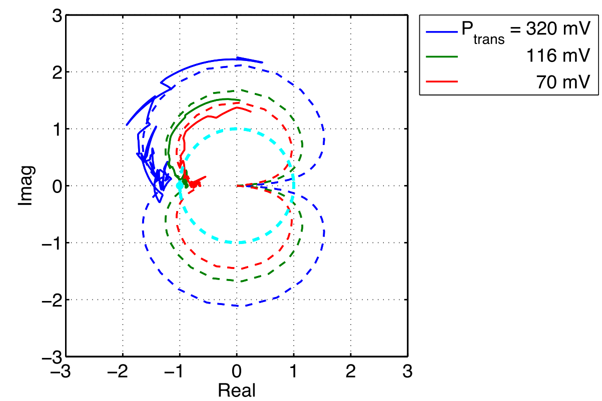


**Fig. 4.** Nyquist plots of $G_{\rm EML}$ at three laser powers. The thin dotted lines are theoretical curves based on Eq. (5) and the thick dotted circle represents the unit circle. The solid lines are determined by the measured data shown in Fig. 6. Note that, in this plot, the moving radius is defined as $\log_{10}(|G_{\rm EML}|) + 1$ ($|G_{\rm EML}| \geq 0.1$), 0 ($|G_{\rm EML}| < 0.1$) for readability. The intracavity power, $P_{\rm int}$, is determined by dividing the transmitted power, $P_{\rm trans}$, by the calibration constant $5.0 \pm 0.1$ W/V [24].

where $E_{\rm DC}$ is the electric circuit's DC gain which can be adjusted by the variable resistance in the electric circuit, and $f_{\rm a} = 1.592$ Hz and $f_{\rm b} = 33.18$ Hz, $f_{\rm c} = 160.2$ Hz are the frequencies of the zero and the two poles, respectively [21]. The sensitivity of the QPD is $S_{\rm QPD} = 142.9\ V_{\rm sum}$ V/m, where $V_{\rm sum}$ is the output voltage of the sum signal of the QPD.

### *3.2. Critical intracavity power making the cavity unstable*

In terms of the equation of rotational motion, Eq. (1), the critical intracavity power, which is the upper limit power for stable operation of the cavity without any angular control system, is defined as $P_{\rm crit} \equiv c k_{\rm mech}/(2\mathcal{L} g_{\rm F})$. When the intracavity power is larger than the critical power, the angular optical anti-spring effect, $k_{\rm RP}$, is larger than the mechanical spring effect of the end mirror, $k_{\rm mech}$. In our experimental setup, $P_{\rm crit}$ is 0.8 W.

The critical power can be explained rather intuitively by Nyquist plots of the control system, which are useful for discussing whether a system is stable or unstable. Now, let us consider the end mirror loop gain, in other words the open loop gain of the lower loop in the block diagram shown in Fig. 2, which is given by

$$G_{\rm EML} = -G_{\rm E}(R_{\rm F} - L) F_{\rm RP} \tag{5}$$

$$\left(\frac{\theta_{\rm E}}{T_{\rm E}}(G_{\rm FB} = 0) = \frac{G_{\rm E}}{1 - G_{\rm E}(R_{\rm F} - L)F_{\rm RP}} \equiv \frac{G_{\rm E}}{1 + G_{\rm EML}}\right). \tag{6}$$

Here, the sign of $G_{\rm EML}$ is defined in Eq. (6). In other words, when the feedback loop is positive feedback, the sign of the open loop gain is defined to be negative. The Nyquist plots of $G_{\rm EML}$ at various intracavity powers are shown in Fig. 4. According to this figure, the feedback system with an intracavity power larger than 0.8 W is unstable because the plot of $G_{\rm EML}$ with an intracavity power larger than 0.8 W encircles the point at $(-1, 0)$.

According to the above discussion, $G_{\rm EML}$ should be measured to observe the angular instability of the cavity, Although $G_{\rm EML}$ cannot be measured directly when the cavity is unstable, $G_{\rm EML}$ can be determined by measurement of the transfer function from $V_{\rm MON}$

**Table 1**
Properties of the cavity and its components. The moment of inertia (MoI) of the end mirror is defined for an axis of rotation passing through the center of the end mirror and perpendicular to the optical axis of the end mirror.

| End mirror | | | | | Front mirror | | | Cavity | |
|---|---|---|---|---|---|---|---|---|---|
| Mass | Diameter | Thickness | MoI | RoC | Mass | Diameter | RoC | Length | Finesse |
| 23 mg | 3 mm | 1.5 mm | $1.7 \times 10^{-11}$ kg m$^2$ | $\infty$ (flat) | 55 g | 2.54 cm | 1 m | 14 cm | 1300 |

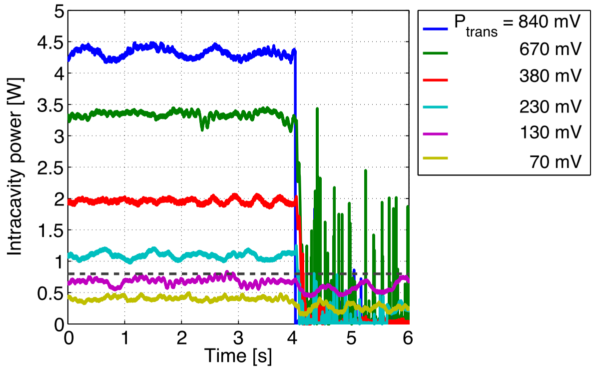


**Fig. 5.** Time series data of the intracavity power at six laser powers. The solid lines are measured data. The dotted line represents the critical intracavity power, 0.80 W. At 4 seconds, the yaw-mode control is turned off.

to $\delta r$ in Fig. 2. This is because the transfer function from $V_{\rm MON}$ to $\delta r$ is obtained as

$$\frac{\delta r}{V_{\rm MON}} = -A_{\rm F} G_{\rm F} R_{\rm F} \frac{1}{1+G_{\rm EML}}, \tag{7}$$

and all terms except $G_{\rm EML}$ in right-hand side of Eq. (7), i.e. $A_{\rm F}$, $G_{\rm F}$, and $R_{\rm F}$ are known. We measured $\delta r/V_{\rm MON}$ at several intracavity powers by exciting the yaw mode of the front mirror by $V_{\rm EXT}$.

### 3.3. Demonstrating the mitigation of the angular instability

For demonstrating the mitigation of angular instability, we need to confirm the stable operation of the cavity under the high laser power condition. Moreover, it should be confirmed that, under this laser power condition, the cavity is indeed unstable without the angular control system because of the radiation-pressure-induced angular instability.

One way to demonstrate the mitigation of the angular instability of the cavity is measuring the time series data of the intracavity power with and without the angular feedback control. The cavity storing an intracavity power higher than the critical power with the angular control system cannot be operated if the angular control system does not work well. On the other hand, the cavity only storing an intracavity power lower than the critical power can be operated even without the angular control system. If this feature of the cavity operation in the time series data depending on the intracavity power is observed, the mitigation of the angular instability is indicated.

Another way to demonstrate the mitigation of the angular instability is observing $G_{\rm EML}$ with the feedback angular control. According to the discussion in Sec. 3.2, if the Nyquist plot of $G_{\rm EML}$ measured with the angular control encircles the point, $(-1, 0)$, the cavity would be unstable without the angular control. In this way, whether the cavity is stable or unstable can be decided without the intracavity power measurement.

## 4. Results and discussion

At six different laser powers, the transmitted lights $P_{\rm trans}$, which correspond to the intracavity powers, were measured in time series data as shown in Fig. 5. At each laser power, $E_{\rm DC}$ was adjusted to keep almost the same DC gain of the angular control loop, which is defined as $G_{\rm FML} \equiv G_{\rm FB} G_{\rm F} R_{\rm F}$. The value of $E_{\rm DC}$ for each laser power is shown in Table 2. In Fig. 5, the yaw-mode control is turned off at 4 seconds. When the yaw-mode control is turned off, the intracavity power is reduced to almost 0 V, which indicates that the lock of the cavity is lost, if the intracavity power is higher than 0.8 W before 4 seconds. If the intracavity power is less than 0.8 W, the cavity remains locked even after the control system is turned off, although the fluctuation of the intracavity power becomes larger.

**Table 2**
Values of $E_{\rm DC}$ at each laser power in the time-series measurement.

| $P_{\rm trans}$ (mV) | 870 | 670 | 380 | 230 | 130 | 70 |
|---|---|---|---|---|---|---|
| $E_{\rm DC}$ | 3.83 | 3.06 | 4.59 | 6.43 | 11.1 | 25.2 |

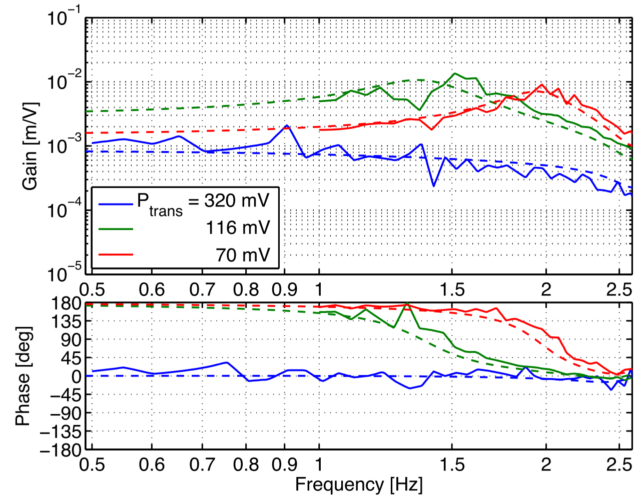


**Fig. 6.** Transfer functions from $V_{\rm MON}$ to $\delta r$ at three laser powers. The solid lines are measured data and the dotted lines are theoretical curves based on Eq. (7).

The transfer function $\delta r/V_{\rm MON}$ was measured at three different laser powers with yaw-mode control as shown in Fig. 6. In this transfer function measurement, $E_{\rm DC}$ was adjusted to keep almost the same DC gain of $G_{\rm FML}$. The values of $E_{\rm DC}$ at $P_{\rm trans} = 320$ mV, 116 mV, and 72 mV were 0.612, 1.15, and 3.83, respectively.

From Fig. 6 and Eq. (7), $G_{\rm EML}$ can be determined in terms of Nyquist plot as shown in Fig. 4. This Nyquist plot of $G_{\rm EML}$ at $P_{\rm trans} = 320$ mV encircles the point $(-1, 0)$, while the other two data at $P_{\rm trans} = 116$ mV, and 70 mV do not encircle the point $(-1, 0)$. Thus, Fig. 4 indicates that, without the yaw-mode control, the cavity would be unstable if the intracavity power would be larger than 0.8 W.

Fig. 5 indicates that the cavity which has the intracavity power larger than the critical power can be operated with the angular control system and is no longer stable without the angular control system. Fig. 4 indicates that, with the angular control system, the cavity is operated stably under the condition where the cavity would be unstable without the angular control system. Therefore, Figs. 4, and 5 show that the radiation-pressure-induced angular instability of the cavity is successfully mitigated by the angular control system using radiation pressure.

## 5. Conclusion

The mitigation of the radiation-pressure-induced angular instability of the Fabry–Perot cavity consisting of suspended mirrors with the angular control system using radiation pressure was successfully demonstrated. In other words, with the angular control system using radiation pressure, the Fabry–Perot cavity consisting of suspended mirrors could be operated under the high laser power condition where we confirm that the cavity would be unstable without the angular control system. Thus, the possibility that the system which could be unstable originally cannot be made stable by some unexpected mechanisms has been negated. This demonstration of mitigating the angular instability of the cavity indicates that the angular control system allows us to increase the intracavity power up to the level required for observing the radiation pressure noise [15].

The angular control system can be used even if only one of the mirrors has an electro-magnetic actuator. Our result in this paper leads to the stable operation of the high-finesse cavity consisting of the suspended tiny mirror for the measurement limited by radiation pressure noise and for demonstrating the quantum non-demolition measurement [15]. In addition, this angular control system using radiation pressure can also be applied to various experiments using a mirror which is affected by the radiation pressure and to which conventional actuators cannot be attached because of spatial constraints or the requirement of a very high mechanical Q value, for example experiments in optical levitation [26].

## Acknowledgements

We thank S. Sakata, D. Friedrich, K. Agatsuma, T. Mori, S. Konisho and T. Nishimura for previous work, and K. Craig for English proofreading. This work was supported by MEXT, JSPS Leading-edge Research Infrastructure Program, JSPS Grant-in-Aid for Specially Promoted Research 26000005, MEXT Grant-in-Aid for Scientific Research on Innovative Areas 24103005, JSPS Core-to-Core Program, A. Advanced Research Networks, JSPS KAKENHI Grant Numbers 23340077 and 26287038, and the joint research program of the Institute for Cosmic Ray Research, University of Tokyo.

## References

[1] J. Aasi, et al., Advanced LIGO, Class. Quantum Gravity 32 (7) (2015) 074001, http://dx.doi.org/10.1088/0264-9381/32/7/074001.

[2] F. Acernese, et al., Advanced Virgo: a second-generation interferometric gravitational wave detector, Class. Quantum Gravity 32 (2) (2015) 024001, http://dx.doi.org/10.1088/0264-9381/32/2/024001, arXiv:1408.3978.

[3] B. Willke, et al., The GEO-HF project, Class. Quantum Gravity 23 (8) (2006) S207–S214, http://dx.doi.org/10.1088/0264-9381/23/8/S26.

[4] Y. Aso, Y. Michimura, K. Somiya, M. Ando, O. Miyakawa, T. Sekiguchi, D. Tatsumi, H. Yamamoto, Interferometer design of the KAGRA gravitational wave detector, Phys. Rev. D 88 (4) (2013) 043007, http://dx.doi.org/10.1103/PhysRevD.88.043007.

[5] B.P. Abbott, et al., Observation of gravitational waves from a binary black hole merger, Phys. Rev. Lett. 116 (6) (2016) 61102, http://dx.doi.org/10.1103/PhysRevLett.116.061102, arXiv:1602.03837.

[6] H. Grote, K. Danzmann, K.L. Dooley, R. Schnabel, J. Slutsky, H. Vahlbruch, First long-term application of squeezed states of light in a gravitational-wave observatory, Phys. Rev. Lett. 110 (18) (2013) 181101, http://dx.doi.org/10.1103/PhysRevLett.110.181101.

[7] J. Aasi, et al., Enhanced sensitivity of the LIGO gravitational wave detector by using squeezed states of light, Nat. Photonics 7 (8) (2013) 613–619, http://dx.doi.org/10.1038/nphoton.2013.177, arXiv:1310.0383v1.

[8] O. Miyakawa, et al., Measurement of optical response of a detuned resonant sideband extraction gravitational wave detector, Phys. Rev. D 74 (2) (2006) 022001, http://dx.doi.org/10.1103/PhysRevD.74.022001.

[9] T. Corbitt, D. Ottaway, E. Innerhofer, J. Pelc, N. Mavalvala, Measurement of radiation-pressure-induced optomechanical dynamics in a suspended Fabry–Perot cavity, Phys. Rev. A 74 (2) (2006) 021802, http://dx.doi.org/10.1103/PhysRevA.74.021802.

[10] A. Buonanno, Y. Chen, Quantum noise in second generation, signal-recycled laser interferometric gravitational-wave detectors, Phys. Rev. D 64 (4) (2001) 042006, http://dx.doi.org/10.1103/PhysRevD.64.042006, arXiv:gr-qc/0102012.

[11] A. Buonanno, Y. Chen, Signal recycled laser-interferometer gravitational-wave detectors as optical springs, Phys. Rev. D 65 (4) (2002) 042001, http://dx.doi.org/10.1103/PhysRevD.65.042001.

[12] H.J. Kimble, Y. Levin, A.B. Matsko, K.S. Thorne, S.P. Vyatchanin, Conversion of conventional gravitational-wave interferometers into quantum nondemolition interferometers by modifying their input and/or output optics, Phys. Rev. D 65 (2) (2002) 022002, http://dx.doi.org/10.1103/PhysRevD.65.022002, arXiv:gr-qc/0008026.

[13] S. Sakata, S. Kawamura, S. Sato, K. Somiya, K. Arai, M. Fukushima, A. Sugamoto, Development of a control scheme of homodyne detection for extracting ponderomotive squeezing from a Michelson interferometer, J. Phys. Conf. Ser. 32 (2006) 464–469, http://dx.doi.org/10.1088/1742-6596/32/1/071.

[14] V.B. Braginsky, F.Y. Khalili, Quantum nondemolition measurements: the route from toys to tools, Rev. Mod. Phys. 68 (1) (1996) 1–11, http://dx.doi.org/10.1103/RevModPhys.68.1.

[15] S. Sakata, Study of the Reduction of the Radiation Pressure Noise in Gravitational Wave Detectors using the Ponderomotive Squeezing, PhD thesis, Ochanomizu University, 2008.

[16] N. Matsumoto, K. Komori, Y. Michimura, G. Hayase, Y. Aso, K. Tsubono, 5-mg suspended mirror driven by measurement-induced backaction, Phys. Rev. A 92 (3) (2015) 033825, http://dx.doi.org/10.1103/PhysRevA.92.033825.

[17] J.A. Sidles, D. Sigg, Optical torques in suspended Fabry–Perot interferometers, Phys. Lett. A 354 (3) (2006) 167–172, http://dx.doi.org/10.1016/j.physleta.2006.01.051.

[18] E. Hirose, K. Kawabe, D. Sigg, R. Adhikari, P.R. Saulson, Angular instability due to radiation pressure in the LIGO gravitational-wave detector, Appl. Opt. 49 (18) (2010) 3474–3484, http://dx.doi.org/10.1364/AO.49.003474, arXiv:0909.0010.

[19] K.L. Dooley, L. Barsotti, R.X. Adhikari, M. Evans, T.T. Fricke, P. Fritschel, V. Frolov, K. Kawabe, N. Smith-Lefebvre, Angular control of optical cavities in a radiation-pressure-dominated regime: the Enhanced LIGO case, J. Opt. Soc. Am. A 30 (12) (2013) 2618–2626, http://dx.doi.org/10.1364/JOSAA.30.002618.

[20] D. Kelley, J. Lough, F. Mangaña Sandoval, A. Perreca, S.W. Ballmer, Observation of photothermal feedback in a stable dual-carrier optical spring, Phys. Rev. D 92 (6) (2015) 062003, http://dx.doi.org/10.1103/PhysRevD.92.062003.

[21] M. Nakano, Study of Opt-Mechanical Cavity Control for Development of Quantum Noise Reduction in KAGRA Gravitational Wave Detector, Master thesis, University of Tokyo, 2014.

[22] Y. Enomoto, K. Nagano, M. Nakano, A. Furusawa, S. Kawamura, Observation of reduction of radiation-pressure-induced rotational anti-spring effect on a 23 mg mirror in a Fabry–Perot cavity, Class. Quantum Gravity 33 (14) (2016) 145002, http://dx.doi.org/10.1088/0264-9381/33/14/145002.

[23] S. Sakata, O. Miyakawa, A. Nishizawa, H. Ishizaki, S. Kawamura, Measurement of angular antispring effect in optical cavity by radiation pressure, Phys. Rev. D 81 (6) (2010) 022001, http://dx.doi.org/10.1103/PhysRevD.81.064023.

[24] K. Nagano, Y. Enomoto, M. Nakano, A. Furusawa, S. Kawamura, New method to measure the angular antispring effect in a Fabry–Perot cavity with remote excitation using radiation pressure, Phys. Lett. A 380 (9–10) (2016) 983–988, http://dx.doi.org/10.1016/j.physleta.2016.01.007.

[25] R.W.P. Drever, J.L. Hall, F.V. Kowalski, J. Hough, G.M. Ford, A.J. Munley, H. Ward, Laser phase and frequency stabilization using an optical resonator, Appl. Phys., B Photophys. Laser Chem. 31 (2) (1983) 97–105, http://dx.doi.org/10.1007/BF00702605.

[26] G. Guccione, M. Hosseini, S. Adlong, M.T. Johnsson, J. Hope, B.C. Buchler, P.K. Lam, Scattering-free optical levitation of a cavity mirror, Phys. Rev. Lett. 111 (18) (2013) 183001, http://dx.doi.org/10.1103/PhysRevLett.111.183001, arXiv:1307.1175.